



Heating Method Effect on SnO Micro-Disks as NO₂ Gas Sensor

Mateus G. Masteghin^{1,2}, Denis R. M. Godoi² and Marcelo O. Orlandi^{2*}

¹ Advanced Technology Institute, University of Surrey, Guildford, United Kingdom, ² Department of Physical-Chemistry, São Paulo State University, Araraquara, Brazil

There is an increasing concern about NO_x emission, and many studies have been carried out using metal oxide semiconductors (MOS) aiming its detection. Among the MOS, the SnO micro-disks present a high sensor response and a great selectivity toward NO₂. Nevertheless, sensor signal, limit of detection (LOD), and recovery time are related to the experimental setup used to carry on the measurements. Thus, two different heating methods (*self-heating* and *external heating*) have been carried out to understand in what manner they change the sensor properties of the SnO micro-disks onto interdigitated electrodes. The *external heating* method presented higher sensor signal, best LOD, and lower recovery time, mainly due to the lack of a temperature gradient between the SnO disks and the chamber atmosphere. On the other hand, response time was shown to be the same regardless of the method. Briefly, the authors used thermodynamic equations to better understand the temperature effect on the gas-solid interactions occurring between SnO disks and NO₂ species.

OPEN ACCESS

Edited by:

Xiaogan Li,

Dalian University of Technology, China

Reviewed by:

Yueli Liu,

Wuhan University of
Technology, China

Peng Sun,

Jilin University, China

*Correspondence:

Marcelo O. Orlandi

marcelo.orlandi@unesp.br

Specialty section:

This article was submitted to
Functional Ceramics,
a section of the journal
Frontiers in Materials

Received: 17 May 2019

Accepted: 01 July 2019

Published: 16 July 2019

Citation:

Masteghin MG, Godoi DRM and
Orlandi MO (2019) Heating Method
Effect on SnO Micro-Disks as NO₂
Gas Sensor. *Front. Mater.* 6:171.
doi: 10.3389/fmats.2019.00171

Keywords: SnO, gas sensor, heating mode, *self-heating*, *external heating*, NO₂

INTRODUCTION

Human activities such as the use of mobile sources and electric power plants are major contributors that generate NO₂, which is one of the compounds in the NO_x family (Nagase and Funatsu, 1990; Correa, 1993). In addition to the intrinsic toxicity of the NO₂ (Azoulay-Dupuis et al., 1983) and its eutrophication aptitude (Glibert et al., 2005), the NO₂ reacts with other molecules in the atmosphere giving rise to acid rain and O₃ (likewise toxic in the troposphere) (Rietjens et al., 1986; Chang et al., 1988). Furthermore, among the NO_x species, NO₂ has the longest lifespan making it difficult to control as this causes spreading (Crutzen, 1979). In this context, there is a need to use highly sensitive and selective gas sensor devices for the detection of this pollutant.

Gas sensor devices based on chemo-resistive metal oxide semiconductors (MOSs), (Barsan and Weimar, 2001; Comini et al., 2002; Barsan et al., 2007; Lee, 2009; Wang et al., 2010; Jin et al., 2017) such as SnO₂ (Batzill and Diebold, 2005; Ren et al., 2015; Xu et al., 2015; Cheng et al., 2016; Kida et al., 2016; Li et al., 2016), ZnO (Xu et al., 2000; Wan et al., 2004; Li et al., 2017; Morandi et al., 2017), In₂O₃ (Li et al., 2003; Zhang et al., 2004; Xiao et al., 2017), WO₃ (Li et al., 2004; Yang and Guo, 2017), and CuO (Kim and Lee, 2014), are widely used for the detection of toxic and explosive gases (NO₂, CO, CH₄, H₂S, and H₂) as well as VOCs (C₃H₆O, and C₂H₅OH). The detection mechanism of these MOSs is based on the resistivity change after the interaction of the analyte gas with the surface of the material, either by direct (NO₂) or indirect (H₂, CO, CH₄) mechanisms (Barsan and Weimar, 2001; Batzill and Diebold, 2005). Among the cited MOSs, SnO₂ has been studied the most, due to its great performance and chemical stability (Batzill and Diebold, 2005). However, more attention has recently been given to other Sn_xO_y stoichiometries with less

stable oxidation states, such as SnO (Suman et al., 2013, 2015; Hien and Heo, 2016; Masteghin and Orlandi, 2018) and Sn₃O₄ (Suman et al., 2014, 2015; Li et al., 2015; Liu et al., 2016).

These unusual stoichiometries were reported as gas sensors, nevertheless, many studies with respect to their sensor mechanism must be performed in order to understand the causes of the high sensor signals, especially regarding NO₂. Suman et al. (2013) reported a giant chemo-resistance of SnO disk-like structures when exposed to 100 ppm of NO₂, achieving a sensor signal of 1,000 (with high selectivity toward H₂, CO, and CH₄), which was attributed to the existence of the lone pairs in the (0 0 1) surface planes (Le Bellac et al., 1995; Walsh and Watson, 2004). Considering the performance of the SnO micro-disks as a gas sensor, this study used the same material, aiming to further understand the gas-solid interactions using different experimental setups.

In summary, this work compares the gas sensor signal of the SnO micro-disks when subjected to distinct experimental arrangements, such as different types of heating. For example, when heated through power controlled external resistors in a horizontal tubular furnace or in a specially designed gas sensor chamber, or else when the measurements were performed through the *self-heating* method. The 1,000-fold increase in the SnO disks resistance is observed when the measurement is performed in the horizontal tubular furnace (Suman et al., 2013) and the lowest recorded sensor signal is observed through the *self-heating* method. The main contribution of this work is to correlate the gas sensor properties to the measurement setup.

EXPERIMENTAL

In order to synthesize the SnO disks, SnO₂ powder (Sigma-Aldrich, 99.9% purity), was mechanically mixed with carbon black (Union Carbide, >99% purity) in a molar ratio of 1.5:1 and submitted to the carbothermal reduction route (Suman et al., 2013; Masteghin and Orlandi, 2018). The procedure involved preparing 1 g of the SnO₂:C mixture that was inserted in the central region of a horizontal tubular furnace, and held at 1,135°C for 75 min using heating and cooling rates of 10°C min⁻¹. A nitrogen flow of 150 cm³ min⁻¹ was used throughout the synthesis in order to maintain an inert atmosphere inside the tube. A dark-colored wool-like material was removed from the alumina tube (cold region) containing a mixture of SnO nanobelts and micro-disks. The mixture was submitted to a separation process in order to decant the SnO micro-disks, which were the subject of this study.

The morphological characteristics of materials were studied in a JEOL (model JSM-7500F) field emission scanning electron microscope (FEG-SEM) and a FEI Dual Beam Microscope (model Helios Nanolab 600i).

The phase and the crystallinity of the SnO disks were analyzed by X-ray diffraction (XRD) using Cu K α radiation ($\lambda = 15,406 \text{ \AA}$) and a D/tEX Ultra two linear detector in a Rigaku (model RINT2000) diffractometer. Raman spectroscopy was performed to study the surface structural variations and the presence of intermediate phases. Micro-Raman scattering spectroscopy was

carried out using a 514 nm laser (Melles Griot) coupled to an iHR550 Horiba module with the microscope head adapted by Jobin Yvon (model M.F.O.).

Gas sensor measurements were performed after small drops (0.5 μL each) of a SnO micro-disks suspension were dropped onto the platinum interdigitated electrodes deposited over alumina substrates.

Meant for the *self-heating* measurements, a built-in-electrode consisting of an interdigitated electrode (IDE) and a heater circuit was used (**Figure 1A**). The heater circuit is made of platinum deposited by sputtering on the back of the substrate. Then, the built-in-electrode containing the SnO disks was inserted in the gas sensor chamber to carry out the measurements.

In order to perform the gas sensor measurements using the *external heating* method, an external resistance present in the sensor chamber heats the SnO sample placed on the gray ceramic piece depicted in **Figure 1B**. Therefore, only the IDE part of the substrate (**Figure 1A**) was used during this kind of measurement. Moreover, the heater warms the whole test chamber (including the analyte) by means of both conduction and convection.

Figure 1C shows another experimental setup previously used to carry on gas sensor measurements heated by the *external heating* method. The details of the horizontal tubular furnace arrangement used to study the SnO micro-disks can be seen in the work of Suman et al. (2013), but a schematic draw is presented in **Figure 1C**. Comparing **Figures 1B,C**, it can be observed that the main difference between the two setups is the larger warm area provided by the external heater of the tubular furnace.

The gas sensor measurements were fixed at 200°C for the *external heating* (conventional heating), the temperature at which the SnO micro-disks presented higher sensor response (Suman et al., 2013). The *self-heating* mode measurements were carried out at 150, 200, and 250°C.

The measurements were carried out by monitoring changes in resistance using a stabilized voltage source (Agilent 34972A) during cyclic exposures to different concentrations of NO₂ (1–50 ppm) diluted in synthetic dry air (baseline gas) using mass flow controllers (MKS). The sensor signal was evaluated by considering the $R_{\text{NO}_2}/R_{\text{Baseline}}$ ratio. The controlled release of the analyte gas (NO₂) at its different concentrations was done after 12 h stabilization of device in dry synthetic air baseline; each NO₂ concentration was released for 20 min at intervals of 1 h between successive releases. The flow remained constant and equal to 200 cm³ min⁻¹ all over the measurements.

RESULTS AND DISCUSSION

A dark brown material was removed from the alumina tube after synthesis. The desired SnO material was sited in a region where the temperature range was between 200 and 350°C.

Figures 2A,B show FEG-SEM images of the SnO micro-disks obtained after the decantation process, showing that the disks and nanobelts were well-separated. It is clearly visible in **Figure 1B** that many of the disks appear to be the

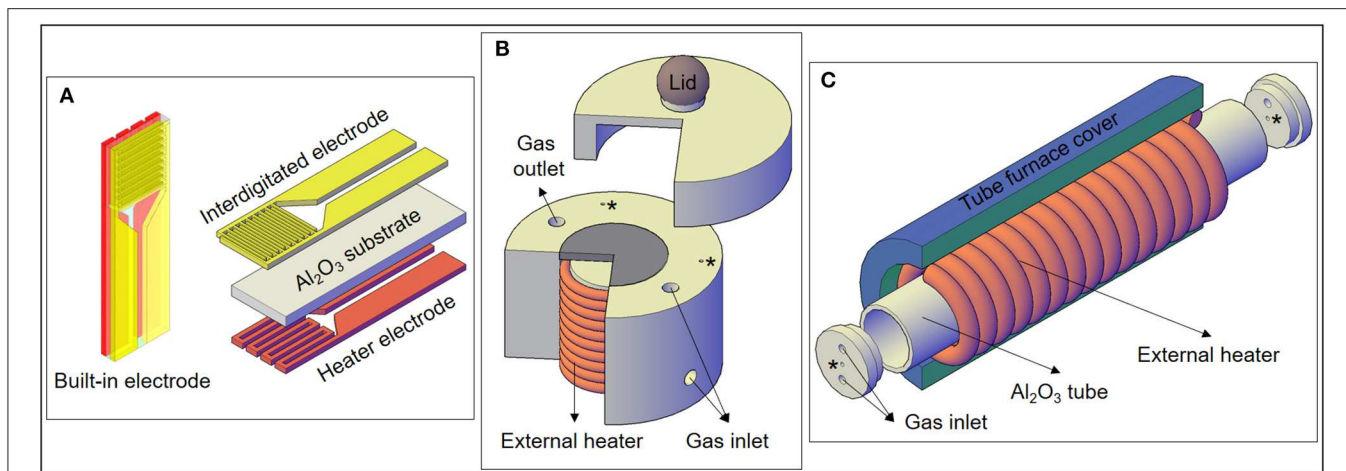


FIGURE 1 | (A) Electrodes used for the experiments, including the heater electrode for the *self-heating* method. **(B)** Specially designed gas sensor chamber used for the *external heating* measurements of this work, with a cross-section showing the external heater. **(C)** Representation of the *external heating* setup used in a previous experiment with SnO micro-disks (Suman et al., 2013). The “**” correspond to wires feedthroughs.

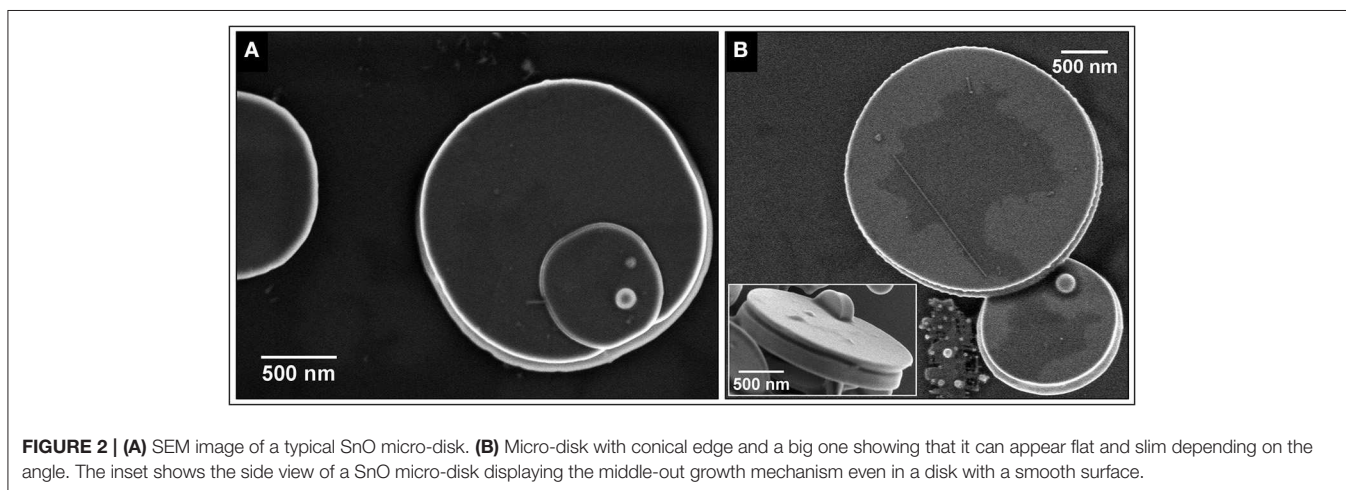


FIGURE 2 | (A) SEM image of a typical SnO micro-disk. **(B)** Micro-disk with conical edge and a big one showing that it can appear flat and slim depending on the angle. The inset shows the side view of a SnO micro-disk displaying the middle-out growth mechanism even in a disk with a smooth surface.

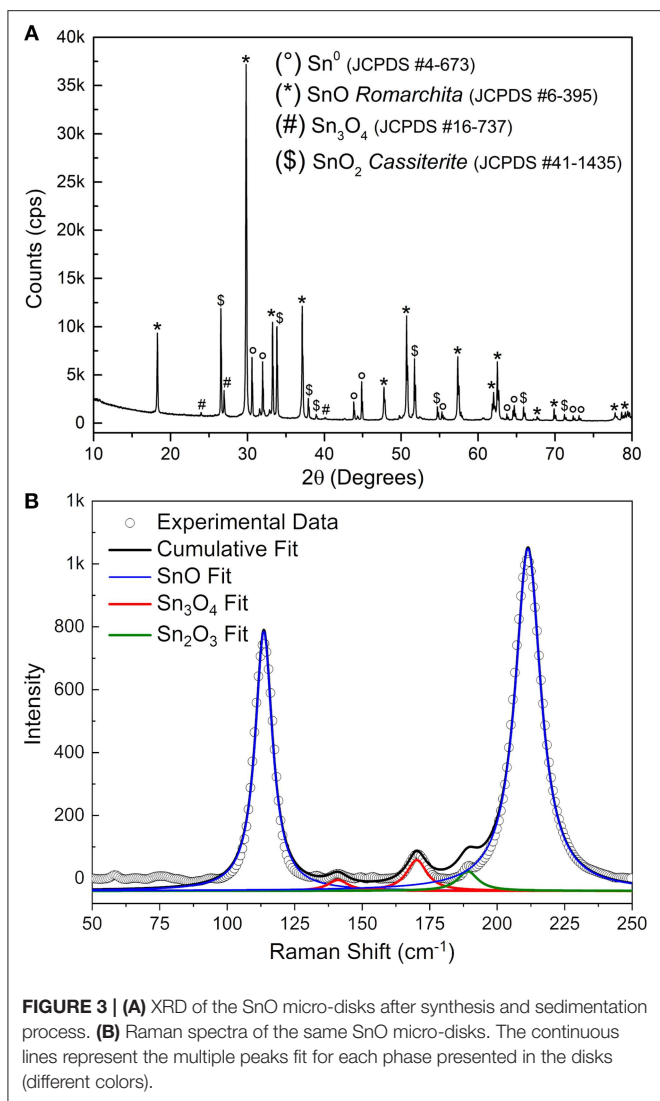
result of two disks stuck together, being this morphological feature related to the vapor-solid (VS) growth mechanism (Dai et al., 2002; Orlandi et al., 2008).

The FEG-SEM images (**Figure 2**) show the existence of at least two phases—disk itself and the bright spheres. Further characterization by XRD (**Figure 3A**) indicates the predominance of the *Romarchite* phase of the SnO (Space group $P4/nmm$, *Litharge*-type Tetragonal structure, similar to α -PbO), nonetheless secondary phases corresponding to the metallic tin (Sn^0) and *cassiterite* phase of the SnO_2 (*Rutile*-type Tetragonal structure) were also indexed as minor amount. A small amount of Sn_3O_4 phase cannot be discarded from the XRD results. For TEM and XANES characterizations, one can refer to the work of Suman et al. (2013).

Figure 3B shows the Raman spectra of the SnO micro-disks alongside the peaks fitting of each present phase. The blue line shows the peaks fit for the SnO phase. The means (χ_c) of the Lorentz simulations are at 113 and 210 cm^{-1} , corresponding to

the E_{1g} and A_{1g} vibrational modes of the SnO phase, respectively. These two χ_c values are somewhat shifted to smaller Raman values compared to the theoretical results (Eifert et al., 2017), as can be seen in **Table 1**.

The existence of the secondary Sn_3O_4 phase (red line) is minor but still present in the Raman measurements, since its A_g vibrational mode appears at 141 cm^{-1} , and the B_g vibrational mode is shown at 170 cm^{-1} . Nevertheless, through Raman measurements, it was also possible to attribute the existence of the Sn_2O_3 phase (green line)—or most probably clusters with this coordination—in the SnO micro-disks (B_g vibrational mode at 189 cm^{-1}). This peak at 189 cm^{-1} and the absence of peaks regarding the SnO_2 phase makes Raman spectroscopy complementary to the XRD, because in the Raman analysis the local bonding and the electronic structure play the main role, in contrast to the XRD, in which only the symmetry, the long-range 3D arrangements, and the atomic factors are taken into account (Sangaletti et al., 1998; Eifert et al., 2017). Besides, theoretical



studies showed that the Sn₂O₃ is the strongest Raman scatterer—and that is the most probable reason it was detected—followed by SnO, Sn₃O₄, and SnO₂ (Eifert et al., 2017).

Comparing the redshift results for the SnO peaks it can be said that the experimental bond lengths are longer than the ones used for the theoretical simulations (Hardcastle and Wachs, 1991). This outcome supports the existence of the lone pairs localized in the Sn²⁺ ions in the tetragonal structure of the SnO (Walsh and Watson, 2004). One noteworthy point is the higher redshift of the A_{1g} mode compared to the E_{1g} mode of the SnO, endorsing the contribution of the lone pairs for increasing the Sn-O binding length, once the A_{1g} mode coincides to the oxygen vibration in the c direction and the E_{1g} corresponds to the atoms vibration perpendicular to the c direction (Geurts et al., 1984). This finding paves the way for a more sophisticated *in-situ* and operando spectroscopy which can detect the interaction of oxidizing molecules (O₂ and NO₂, for example) with the SnO lone pairs, by shifting the peaks at 113 and 210 cm⁻¹

to higher wavenumbers values, since an interacting molecular orbital causes less repulsion to the surrounding atoms rather than a lone pair (Atkins et al., 2018).

Figure 4A shows the gas sensor response of the SnO micro-disks under three different temperatures reached via the *self-heating* method. One can see the higher sensor signal obtained at 200°C (except for 1 ppm of NO₂), as expected based on the measurements carried out in an adapted tubular furnace (Suman et al., 2013). This result emphasizes the need for a balance between the adsorption and desorption rate of the gases onto the SnO surface—both exponentially reliant on the temperature. Equation 1 shows an easier way of understanding this temperature effect on the sensor signal only by means of surface coverage (Θ):

$$\Theta = \frac{k_{ads}}{k_{des}} * \exp \frac{\Delta H_{Chem}}{kT}, \quad (1)$$

where k_{ads} and k_{des} are the adsorption and desorption constants, respectively; ΔH_{Chem} is the chemisorption enthalpy; k is the Boltzmann constant; and T is the temperature in Kelvin.

It is well-known that some amount of energy (heat) is necessary to overcome the activation barrier for the chemisorption (ΔH_{Chem}), otherwise, the gas molecules would be in a physisorbed state (Batzill and Diebold, 2005). However, by Equation 1, if the temperature goes too high the coverage decreases and sensor signal drops, in full agreement with previous results involving SnO micro-disks in multi- and single-device configurations (Suman et al., 2013; Masteghin and Orlandi, 2018).

Figure 4B shows the sensor response for the SnO micro-disks at 200°C reached through two different heating modes, *external heating* (red spheres), and *self-heating* (blue triangles). The sensor signal is higher for the device when it is in a hermetically sealed chamber heated by conventional resistances (*external heating*)—equals to 52 at 50 ppm—rather than when *self-heating* method was used—sensor signal equals to nine. Furthermore, the detection limit (LOD) for NO₂ analyte went from 1 ppm using the *self-heating* mode to 600 ppb using the *external heating* method, both below the toxic limits. Despite the different sensor signals obtained for the two samples when exposed to different heating modes, both presented increasing sensor signals as the NO₂ concentration increased. This is a result of the increased values of resistance reached after different concentrations of the analyte gas were released, corresponding to an n-type semiconductor behavior.

Table 2 summarizes the obtained sensor signals for 50 ppm of NO₂, with a constant flow of 200 sccm, at 200°C. Previous results obtained in a horizontal tubular furnace were added in **Table 2** for comparative purposes (Suman et al., 2013).

To understand how the experimental setup influences the gas sensor response is necessary to elucidate the interactions between the surface of the material and the gases (mainly O_x^{y-} species, and NO₂ from the baseline and analyte gas, respectively). The SnO micro-disks deposited onto the IDE will be considered as a porous layer with grain boundaries generated by the contact between the discs. The initial oxygen species that can vary within

TABLE 1 | Obtained peaks mean values (χ_c) for the SnO micro-disks Raman Spectra, and the theoretical results for comparative purposes.

Peak Number	Experimental χ_c	Theoretical (Eifert et al., 2017)
1) E _{1g} SnO	113 cm ⁻¹	115 cm ⁻¹
2) A _g Sn ₃ O ₄	141 cm ⁻¹	140 cm ⁻¹
3) B _g Sn ₃ O ₄	170 cm ⁻¹	170 cm ⁻¹
4) B _g Sn ₂ O ₃	189 cm ⁻¹	190 cm ⁻¹
5) A _{1g} SnO	210 cm ⁻¹	217 cm ⁻¹

TABLE 2 | The gas sensor signals for 50 ppm of NO₂ at 200°C.

Heating mode	Sensor signal
External heating	52
Self-heating	9
Horizontal tubular furnace (Suman et al., 2013)	550

The first two methods were the ones used in this study and the last one was included for a comparative purpose (Suman et al., 2013). All of them used a constant flow of 200 sccm consisting of NO₂ and dry synthetic air mixture.

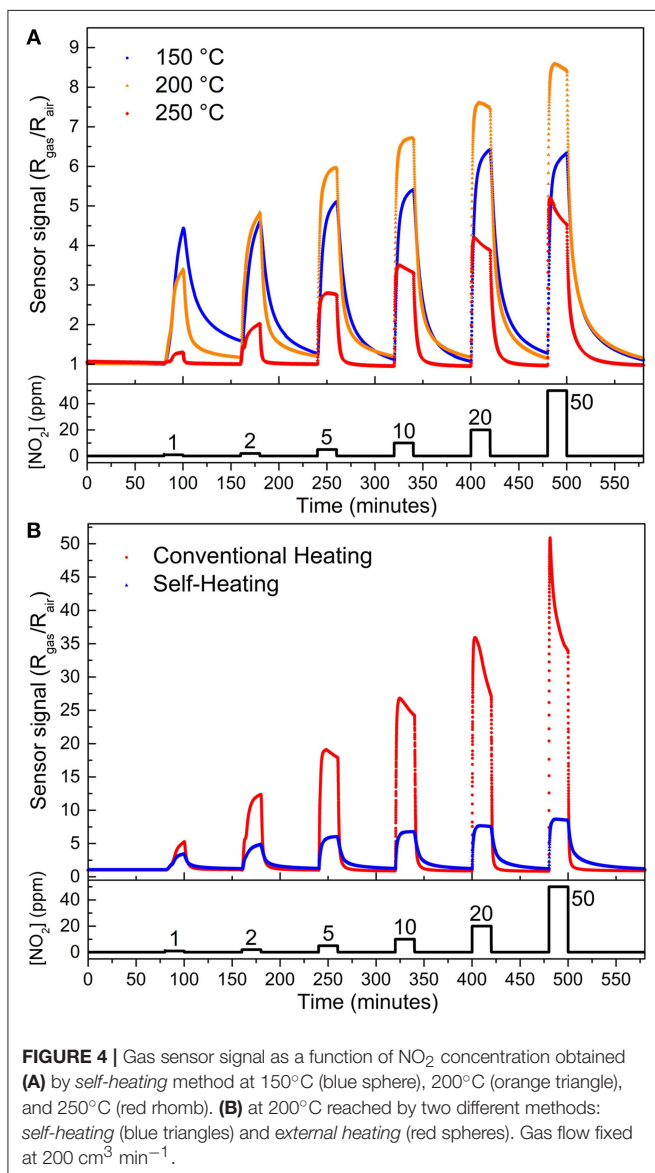


FIGURE 4 | Gas sensor signal as a function of NO₂ concentration obtained (A) by self-heating method at 150°C (blue sphere), 200°C (orange triangle), and 250°C (red rhomb). (B) at 200°C reached by two different methods: self-heating (blue triangles) and external heating (red spheres). Gas flow fixed at 200 cm³ min⁻¹.

the operating temperature adsorb onto the material surface generating back-to-back potential barriers at the boundaries. Afterward, the NO₂ interacts with the empty tin sites through the overlap of NO₂ empty π_u molecular orbital with the (Sn 5s–O 2p_z)^{*} lone pairs, further increasing the resistivity of the material

by heightening and enlarging those potential barriers (Barsan and Weimar, 2001; Batzill and Diebold, 2005).

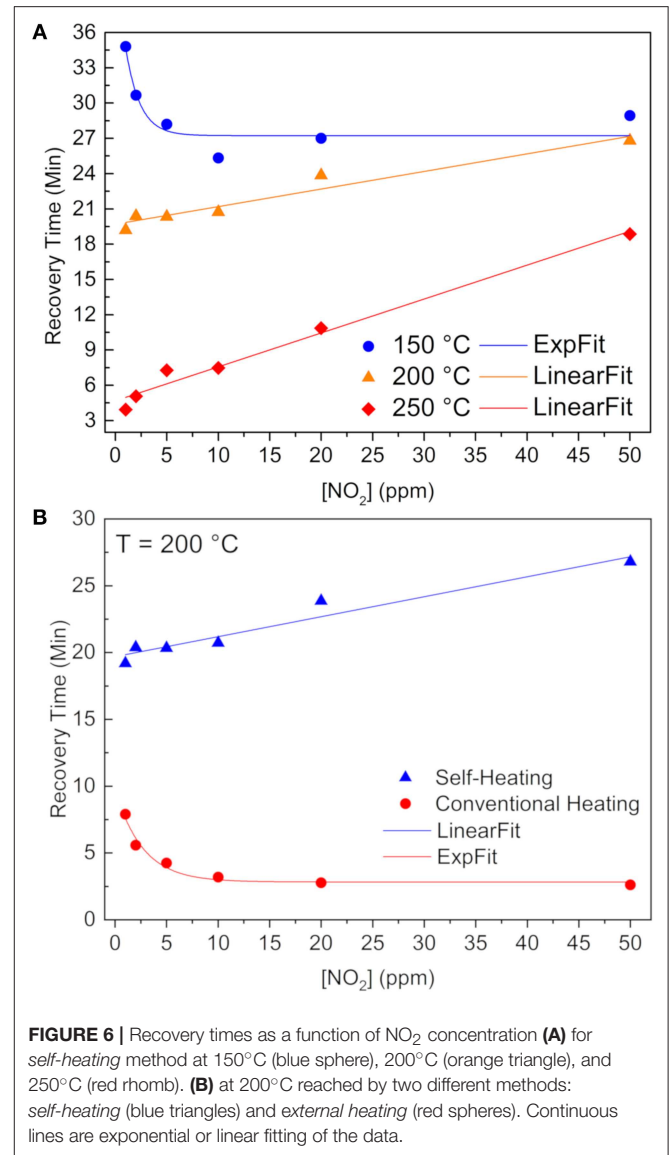
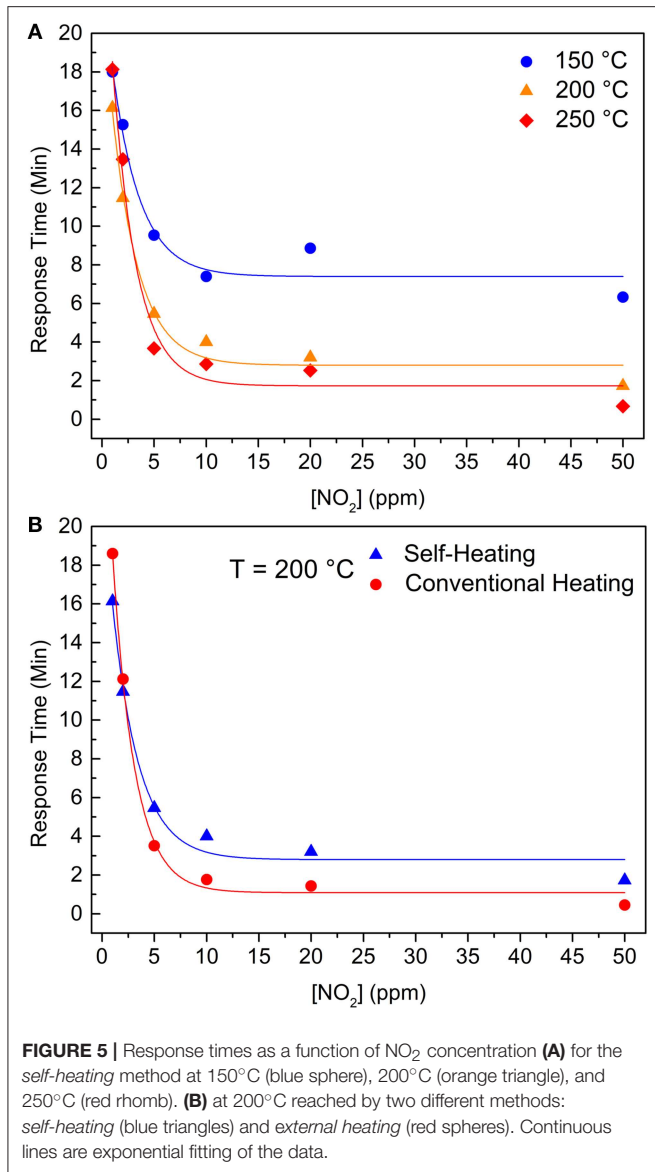
Thus, knowing that NO₂ directly interacts with SnO surface, the higher availability of the analyte will enhance the sensor signal, due to a higher amount of electrons transferred from the semiconductor to the chemisorbed gas. Bearing this in mind, the setup heated by the *external heating* method is the most likely to present a larger sensor signal since it would deliver a greater amount of NO₂ to react with SnO. This occurs because the NO₂ dimerization reaction (Equation 2) is an exothermic reaction which releases (–)57.2 kJ mol⁻¹. Consequently, by the Le Chatelier Principle the heat (temperature) can change the reaction direction to the NO₂ side (Atkins and Jones, 2005).



NO₂ dimerization has a relatively high K_p (equilibrium constant) of 6.5 at 25°C, which decreases to K_p equals 1.18 at 49.5°C (and, ~0.05 at 200°C) (Yu and Gao, 1997), endorsing the temperature effect on the amount of NO₂ delivered to the SnO disks. So, Equation (2) and the K_p values support the *external heating* method presenting a higher sensor signal than the *self-heating* method.

Another factor contributing to the higher sensor signal of the *external heating* mode is the temperature effect (T) on the chemical potential of the NO₂ molecules (μ_{NO_2}) in the vapor phase [$\mu_{\text{NO}_2} = \mu_0 + RT \ln(P_{\text{NO}_2})$]. It takes place because the difference in the chemical potential of the vapor phase and the adsorbed state drives the equilibrium, and once NO₂ molecules have a higher μ_{NO_2} value in the heated chamber, it has a higher probability to form the Sn–NO₂ adsorbed state. Nonetheless, the higher sensor signal obtained in the tubular furnace (Table 2), is related to having a larger room for the analyte gas to be heated before reaching the sample.

Figure 5A shows the response times for the *self-heating* measurements at three different temperatures (150, 200, and 250°C), where an exponential behavior (continuous lines) can be seen in each working temperature. The increasing temperature resulted in smaller response times, especially at higher NO₂ concentration, and this effect is most pronounced between response times at 150 and 200°C. These features indicate an Arrhenius kinetics with a given threshold activation energy for the chemisorption process that is supplied to the material as heat (Zaza et al., 2019). Moreover, Figure 5B shows that different heating methods do not cause a meaningful variation in the response time at 200°C.

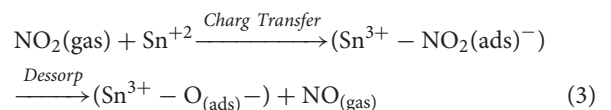


Thus, one can infer that the velocity of resistance change during the gas adsorption/chemisorption is controlled by the energy given to the electrons to cross an electric field of a charged surface (with a dipole momentum), reaching the NO₂ molecule. Once this energy is mainly provided as *heat*, and the temperature close to the IDE is the same for both heating methods, electrons have the same probability of reaching the surface and, consequently, the same response times, regardless being *self-heating* or *external heating*.

From **Figure 6A** one can see a recovery time behavior change whilst increasing the operating temperature throughout the *heater*. In order to have a 90% recovery of the baseline resistance value, chemisorbed NO₂ molecules must be released from the tin atoms. Thus, considering an Arrhenius kinetics for this removal rate constant ($k = A * e^{-\frac{E}{kT}}$), the limiting factor at 200 and 250°C is the pre-exponential factor (A), because at higher IDE

temperatures, the NO₂ are loosely overlapped with the SnO lone pairs, so the required energy (ΔE) does not control the kinetics any longer, but rather the amount of favorable collisions, which are smaller in the *self-heating* system when compared to *external heating* method (Batzill and Diebold, 2005).

Figure 6B clearly shows a lower recovery time when submitted to the *external heating* method, as a result of both higher pre-exponential factor and more energy available. Besides, we showed that O_(ads) species still remain onto the SnO surface, after stopping the release of the NO₂ (Masteghin and Orlandi, 2018), indicated in Equation (3) (Kaur et al., 2007; Sharma et al., 2013):



Thus, having oxygen atomic species (O^-) is the quickest way to withdrawal these $O_{(ads)}$ of the SnO surface and restore the baseline as observed for the *external heating* measurements. It is well-known that oxygen species depend on temperature (Barsan and Weimar, 2001), and that atomic oxygen is the majority at 200°C, in contrast with lower temperatures—like the atmosphere inside the chamber when using the *self-heating* method—where O_2^- are present.

In the present investigation, it has been shown how the experimental setup can influence the obtained gas sensor properties, such as sensor signal, limit of detection, and recovery time. This shows that the sensor signal increases and the recovery time decreases when using the *external heating* method (conventional), and no meaningful effect on the response time was observed when using the *self-heating* mode.

CONCLUSION

The present work has used SnO micro-disks in “carpet” mode, previously proven to be an excellent NO₂ sensor, to show how the experimental setup affects the gas sensor properties. XRD showed a majority of SnO phase (*Litharge*-type tetragonal structure), and this result was endorsed by Raman spectroscopy. Raman was also used to experimentally evince the existence of the so-called *lone pairs*, theoretically predicted and used to explain the high sensor response toward NO₂. Gas sensor measurements have shown that the gradient of temperature between the sample and the chamber atmosphere is responsible for the lower sensor signal obtained by the *self-heating* method, as well as the higher recovery time. Although the former properties have changed with the heating method, the response time was not influenced.

REFERENCES

- Atkins, P., De Paula, J., and Keeler, J. (2018). *Atkins Physical Chemistry*. Oxford, UK: Oxford University Press.
- Atkins, P., and Jones, L. (2005). *Chemical Principles. The Quest for Insight*. New York, NY: W. H. Freeman.
- Azoulay-Dupuis, E., Torres, M., Soler, P., and Moreau, J. (1983). Pulmonary NO₂ toxicity in neonate and adult guinea pigs and rats. *Environ. Res.* 30, 322–339. doi: 10.1016/0013-9351(83)90218-9
- Barsan, N., Koziej, D., and Weimar, U. (2007). Metal oxide-based gas sensor research: how to? *Sens. Actuators B Chem.* 121, 18–35. doi: 10.1016/j.snb.2006.09.047
- Barsan, N., and Weimar, U. (2001). Conduction model of metal oxide gas sensors. *J. Electroceram.* 7, 143–167. doi: 10.1023/A:1014405811371
- Batzill, M., and Diebold, U. (2005). The surface and materials science of tin oxide. *Prog. Surf. Sci.* 79, 47–154. doi: 10.1016/j.progsurf.2005.09.002
- Chang, L.-Y., Mercer, R. R., Stockstill, B. L., Miller, F. J., Graham, J. A., Ospital, J. J., et al. (1988). Effects of low levels of NO₂ on terminal bronchiolar cells and its relative toxicity compared to O₃. *Toxicol. Appl. Pharmacol.* 96, 451–464. doi: 10.1016/0041-008X(88)90005-1
- Cheng, J. P., Wang, J., Li, Q. Q., Liu, H. G., and Li, Y. (2016). A review of recent developments in tin dioxide composites for gas sensing application. *J. Ind. Eng. Chem.* 44, 1–22. doi: 10.1016/j.jiec.2016.08.008
- Comini, E., Faglia, G., Sberveglieri, G., Pan, Z., and Wang, Z. L. (2002). Stable and highly sensitive gas sensors based on semiconducting oxide nanobelts. *Appl. Phys. Lett.* 81, 1869–1871. doi: 10.1063/1.1504867
- Correa, S. M. (1993). A review of NO_x formation under gas-turbine combustion conditions. *Combust. Sci. Technol.* 87, 329–362. doi: 10.1080/00102209208947221
- Crutzen, P. J. (1979). The role of NO and NO₂ in the chemistry of the troposphere and stratosphere. *Annu. Rev. Earth Planet Sci.* 7, 443–472. doi: 10.1146/annurev.ea.07.050179.002303
- Dai, Z. R., Pan, Z. W., and Wang, Z. L. (2002). Growth and structure evolution of novel tin oxide diskettes. *J. Am. Chem. Soc.* 124, 8673–8680. doi: 10.1021/ja026262d
- Eifert, B., Becker, M., Reindl, C. T., Giar, M., Zheng, L., Polity, A., et al. (2017). Raman studies of the intermediate tin-oxide phase. *Phys. Rev. Mater.* 1:14602. doi: 10.1103/PhysRevMaterials.1.014602
- Geurts, J., Rau, S., Richter, W., and Schmitte, F. J. (1984). SnO films and their oxidation to SnO₂: raman scattering, IR reflectivity and X-ray diffraction studies. *Thin Solid Films.* 121, 217–225. doi: 10.1016/0040-6090(84)90303-1
- Glibert, P. M., Seitzinger, S., Heil, C. A., Burkholder, J. M., Parrow, M. W., Codispoti, L. A., et al. (2005). The role of eutrophication in the global proliferation of harmful algal blooms. *Oceanography* 18, 198–209. doi: 10.5670/oceanog.2005.54
- Hardcastle, F. D., and Wachs, I. E. (1991). Determination of vanadium-oxygen bond distances and bond orders by Raman spectroscopy. *J. Phys. Chem.* 95, 5031–5041. doi: 10.1021/j100166a025
- Hien, V. X., and Heo, Y.-W. (2016). Effects of violet-, green-, and red-laser illumination on gas-sensing properties of SnO thin film. *Sens. Actuators B Chem.* 228, 185–191. doi: 10.1016/j.snb.2015.12.105

This work main contribution is the use of basic thermodynamic equations to explain how temperature affects the dimerization equilibrium of NO₂ molecules, the chemical potential of the analyte gas, the material coverage, and the desorption rate constant. Accordingly, the need to detail the experimental arrangement whilst analyzing the sensor properties.

DATA AVAILABILITY

The datasets generated for this study are available on request to the corresponding author.

AUTHOR CONTRIBUTIONS

MM executed the experimental work, wrote the first version of the manuscript, and was involved in the data analysis. DG analyzed the Raman results and revised the manuscript. MO is the coordinator of the research project, revised the manuscript, and worked on electron microscopy and electrical data analysis.

FUNDING

This research was funded by FAPESP [#2013/07296-2, #2015/21033-0, #2017/12870-0, and #2017/26219-0] and CNPq [#447760/2014-9, #303542/2015-2, and #443138/2016-8].

ACKNOWLEDGMENTS

The authors thank LMA-IQ for providing electron microscopy facilities.

- Jin, H., Abu-Raya, Y. S., and Haick, H. (2017). Advanced materials for health monitoring with skin-based wearable devices. *Adv. Healthc. Mater.* 6:1700024. doi: 10.1002/adhm.201700024
- Kaur, J., Kumar, R., and Bhatnagar, M. C. (2007). Effect of indium-doped SnO₂ nanoparticles on NO₂ gas sensing properties. *Sens. Actuators B Chem.* 126, 478–484. doi: 10.1016/j.snb.2007.03.033
- Kida, T., Suematsu, K., Hara, K., Kanie, K., and Muramatsu, A. (2016). Ultrasensitive detection of volatile organic compounds by a pore tuning approach using anisotropically shaped SnO₂ nanocrystals. *ACS Appl. Mater. Interfaces.* 8, 35485–35495. doi: 10.1021/acsami.6b13006
- Kim, H.-J., and Lee, J.-H. (2014). Highly sensitive and selective gas sensors using p-type oxide semiconductors: overview. *Sens. Actuators B Chem.* 192, 607–627. doi: 10.1016/j.snb.2013.11.005
- Le Bellac, D., Kiat, J. M., and Garnier, P. (1995). Electronic lone pair localization and electrostatic energy calculations: application to α -PbO, SnO, Pb_{1-x}(TiO)_xO, Pb₃O₄, Pb₃(V,P)₂O₈, and a BiSrCaCuO-type superconductor. *J. Solid State Chem.* 114, 459–468. doi: 10.1006/jssc.1995.1069
- Lee, J.-H. (2009). Gas sensors using hierarchical and hollow oxide nanostructures: overview. *Sens. Actuators B Chem.* 140, 319–336. doi: 10.1016/j.snb.2009.04.026
- Li, C., Zhang, D., Liu, X., Han, S., Tang, T., Han, J., et al. (2003). In₂O₃ nanowires as chemical sensors. *Appl. Phys. Lett.* 82, 1613–1615. doi: 10.1063/1.1559438
- Li, S.-H., Chu, Z., Meng, F.-F., Luo, T., Hu, X.-Y., Huang, S.-Z., et al. (2016). Highly sensitive gas sensor based on SnO₂ nanorings for detection of isopropanol. *J. Alloys Compd.* 688, 712–717. doi: 10.1016/j.jallcom.2016.07.248
- Li, S.-M., Zhang, L.-X., Zhu, M.-Y., Ji, G.-J., Zhao, L.-X., Yin, J., et al. (2017). Acetone sensing of ZnO nanosheets synthesized using room-temperature precipitation. *Sens. Actuators B Chem.* 249, 611–623. doi: 10.1016/j.snb.2017.04.007
- Li, X., Wang, F., Tu, J., Shah, H. U., Hu, J., Li, Y., et al. (2015). Synthesis and ethanol sensing properties of novel hierarchical Sn₃O₄ nanoflowers. *J. Nanomater.* 16:980170. doi: 10.1155/2015/980170
- Li, X.-L., Lou, T.-J., Sun, X.-M., and Li, Y.-D. (2004). Highly sensitive WO₃ hollow-sphere gas sensors. *Inorg. Chem.* 43, 5442–5449. doi: 10.1021/ic049522w
- Liu, J., Wang, C., Yang, Q., Gao, Y., Zhou, X., Liang, X., et al. (2016). Hydrothermal synthesis and gas-sensing properties of flower-like Sn₃O₄. *Sens. Actuators B Chem.* 224, 128–133. doi: 10.1016/j.snb.2015.09.089
- Masteghin, M., and Orlandi, M. (2018). A gas sensor based on a single sno micro-disk. *Sensors.* 18:3229. doi: 10.3390/s18103229
- Morandi, S., Fioravanti, A., Cerrato, G., Lettieri, S., Sacerdoti, M., and Carotta, M. C. (2017). Facile synthesis of ZnO nano-structures: morphology influence on electronic properties. *Sens. Actuators B Chem.* 249, 581–589. doi: 10.1016/j.snb.2017.03.114
- Nagase, K., and Funatsu, K. (1990). “A study of NO_x generation mechanism in diesel exhaust gas,” in *SAE and Technical Paper* (Warrendale, PA), doi: 10.4271/901615
- Orlandi, M. O., José Ramirez, A., Leite, E. R., and Longo, E. (2008). Morphological evolution of tin oxide nanobelts after phase transition. *Cryst. Growth Des.* 8, 1067–1072. doi: 10.1021/cg7009379
- Ren, H., Zhao, W., Wang, L., Ryu, S. O., and Gu, C. (2015). Preparation of porous flower-like SnO₂ micro/nano structures and their enhanced gas sensing property. *J. Alloys Compd.* 653, 611–618. doi: 10.1016/j.jallcom.2015.09.065
- Rietjens, M., Poelen, C. M., Hempenius, R. A., Gijbels, M. J., and Alink, G. M. (1986). Toxicity of ozone and nitrogen dioxide to alveolar macrophages: comparative study revealing differences in their mechanism of toxic action. *J. Toxicol. Environ. Heal.* 19, 555–568. doi: 10.1080/15287398609530952
- Sangaletti, L., Depero, L. E., Allieri, B., Pioselli, F., Comini, E., Sberveglieri, G., et al. (1998). Oxidation of Sn thin films to SnO₂. Micro-Raman mapping and x-ray diffraction studies. *J. Mater. Res.* 13, 2457–2460. doi: 10.1557/JMR.1998.0343
- Sharma, A., Tomar, M., and Gupta, V. (2013). WO₃ nanoclusters–SnO₂ film gas sensor heterostructure with enhanced response for NO₂. *Sens. Actuators B Chem.* 176, 675–684. doi: 10.1016/j.snb.2012.09.094
- Suman, P. H., Felix, A. A., Tuller, H. L., Varela, J. A., and Orlandi, M. O. (2013). Giant chemo-resistance of SnO disk-like structures. *Sens. Actuators B Chem.* 186, 103–108. doi: 10.1016/j.snb.2013.05.087
- Suman, P. H., Felix, A. A., Tuller, H. L., Varela, J. A., and Orlandi, M. O. (2015). Comparative gas sensor response of SnO₂, SnO and Sn₃O₄ nanobelts to NO₂ and potential interferents. *Sens. Actuators B Chem.* 208, 122–127. doi: 10.1016/j.snb.2014.10.119
- Suman, P. H., Longo, E., Varela, J. A., and Orlandi, M. O. (2014). Controlled synthesis of layered Sn₃O₄ nanobelts by carbothermal reduction method and their gas sensor properties. *J. Nanosci. Nanotechnol.* 14, 6662–6668. doi: 10.1166/jnn.2014.9356
- Walsh, A., and Watson, G. W. (2004). Electronic structures of rocksalt, litharge, and herzenbergite SnO by density functional theory. *Phys. Rev. B Condens. Matter Mater. Phys.* 70:235114. doi: 10.1103/PhysRevB.70.235114
- Wan, Q., Li, Q. H., Chen, Y. J., Wang, T.-H., He, X. L., Li, J. P., et al. (2004). Fabrication and ethanol sensing characteristics of ZnO nanowire gas sensors. *Appl. Phys. Lett.* 84, 3654–3656. doi: 10.1063/1.1738932
- Wang, C., Yin, L., Zhang, L., Xiang, D., and Gao, R. (2010). Metal oxide gas sensors: sensitivity and influencing factors. *Sensors.* 10, 2088–2106. doi: 10.3390/s100302088
- Xiao, B., Wang, D., Song, S., Zhai, C., Wang, F., and Zhang, M. (2017). Fabrication of mesoporous In₂O₃ nanospheres and their ultrasensitive NO₂ sensing properties. *Sens. Actuators B Chem.* 248, 519–526. doi: 10.1016/j.snb.2017.04.022
- Xu, G., Zhang, L., He, C., Ma, D., and Lu, Z. (2015). Adsorption and oxidation of NO on various SnO₂(110), surfaces: a density functional theory study. *Sens. Actuators B Chem.* 221, 717–722. doi: 10.1016/j.snb.2015.06.143
- Xu, J., Pan, Q., and Tian, Z. (2000). Grain size control and gas sensing properties of ZnO gas sensor. *Sens. Actuators B Chem.* 66, 277–279. doi: 10.1016/S0925-4005(00)00381-6
- Yang, F., and Guo, Z. (2017). Different post-treatment processes and different gas sensing behaviors of hierarchical hollow tungsten trioxide shell. *Mater. Lett.* 203, 93–96. doi: 10.1016/j.matlet.2017.05.096
- Yu, Q., and Gao, H. (1997). A simple determination of the NO₂ dimerization equilibrium constant. *J. Chem. Educ.* 74:233. doi: 10.1021/ed074p233
- Zaza, F., Pallozzi, V., and Serra, E. (2019). Optimization of working conditions for perovskite-based gas sensor devices by multiregression analysis. *J. Nanotechnol.* 2019:4628765. doi: 10.1155/2019/4628765
- Zhang, D., Liu, Z., Li, C., Tang, T., Liu, X., Han, S., et al. (2004). Detection of NO₂ down to ppb levels using individual and multiple In₂O₃ nanowire devices. *Nano Lett.* 4, 1919–1924. doi: 10.1021/nl0489283

Conflict of Interest Statement: The authors declare that the research was conducted in the absence of any commercial or financial relationships that could be construed as a potential conflict of interest.

Copyright © 2019 Masteghin, Godoi and Orlandi. This is an open-access article distributed under the terms of the Creative Commons Attribution License (CC BY). The use, distribution or reproduction in other forums is permitted, provided the original author(s) and the copyright owner(s) are credited and that the original publication in this journal is cited, in accordance with accepted academic practice. No use, distribution or reproduction is permitted which does not comply with these terms.